Flow characteristic study of contractions of compressor intermediate S-shaped duct facility

Manish Sharma*, Beena D. Baloni,
Mechanical Engineering, Sardar Vallabhbhai National Institute of Technology,Surat-395007,Gujarat,India
*Corresponding author Email: Sharma.manish726@gmail.com

This paper presents the influence of wall contours on circular cross-section contraction nozzle of compressor intermediate S-shaped duct facility. Flow uniformity and boundary layer development under the different wall contour are examined by using numerical simulations. Effect of wall shape on the pressure loss within the contraction is examined and the maximum difference of pressure loss between the two wall shapes is about 84 Pa. The first derivatives of the wall equations give a sign about the flow quality at the outlet. Higher order equation encounters higher pressure loss due to secondary flow generation and thicker boundary layer development.

***Keywords*:** S-shaped duct, contraction wall shape, CFD

1 Introduction

Commercial aircraft engines Demand lower noise and less specific fuel consumption. Turbofan engine meets these requirements through bypassing some portion of the total air flow from the compressor, combustion chamber, turbine and finally nozzle. Long range civilian engines like GE90, GP7000 and Rolls-Royce Trent 1000 are operated at high bypass ratio of 8-11 to lower the specific fuel consumption. This SFC also helps to improve engine fuel efficiency [1]. Flow has to be directed from low-pressure system to High- pressure system and vice versa through annular ducts with a particular radial offset, hence higher the bypass ratio, larger the radial offset and disk bore diameter [2]. In a twin spool arrangement, interconnecting ducts are used to make flow continuity between the turbo-machinery passages. Besides the compressors, application of the interconnecting ducts can be found in-between various components of the gas turbine which is shown in Fig. Duct connecting the low to the high-pressure compressor is designed with virtually negligible diffusion rate, hence it ceases to constant area ratio (AR) whereas; inter-stage turbine duct shows area variation throughout the passages hence a significant amount of diffusion is taken place[3]. Moreover, optimization and weight penalties dictate that the duct must be as short as possible. Hence, it is designed as an S-shaped and this curved S-shape passage gives rise to the secondary as well as three-dimensionally affects the flow. Therefore a low-speed large-scale experimental rig is designed for studying the flow within the intermediate compressor duct.

Schematic layout of the experimental facility is shown in Fig.2. It consists of a wide-angle diffuser, settling chamber, honeycomb, screens, and contraction nozzle with a bullet, upstream and downstream straight duct and S-shaped annular duct. Compressed air at the required pressure ratio from the screw compressor is supplied to the facility. S-shaped duct plays a vital role to supply the high-quality air to the downstream high-pressure compressor hence; S-shaped itself must be supplied highly uniform air from the upstream components. The contraction nozzle placed upstream to the S-shaped duct has taken this responsibility. As soon as the compressed air approaches to the contraction nozzle, its mean velocity gets increased which allow putting the honeycomb and screens into a low-speed region that help to reduce the pressure losses. Moreover, it also mitigates both mean and fluctuating velocity variations to a smaller fraction of the average velocity. The design of the contraction is significantly affected by the contraction ratio, contraction length, and contraction wall contour [4]. The optimum value of the contraction ratio and length are always desired to minimize the boundary layer thickness, overall cost, and to avoid the flow

separation. Contraction ratio in between 6 to 9 is generally supposed to produce an acceptable flow quality [5]. In the present case, the contraction ratio of 9 is taken. Moreover, the contraction wall shape also affects the performance of the contraction in terms of pressure drop and boundary layer evolution hence several researchers had been focusing towards especially since the last two decades [6-7].

The aim of the present work is to carry out numerical simulations using Ansys FLUENT to analyze the performance of the circular contraction nozzle in terms of pressure drop, exit flow uniformity and boundary layer thickness for four different wall contour shapes.

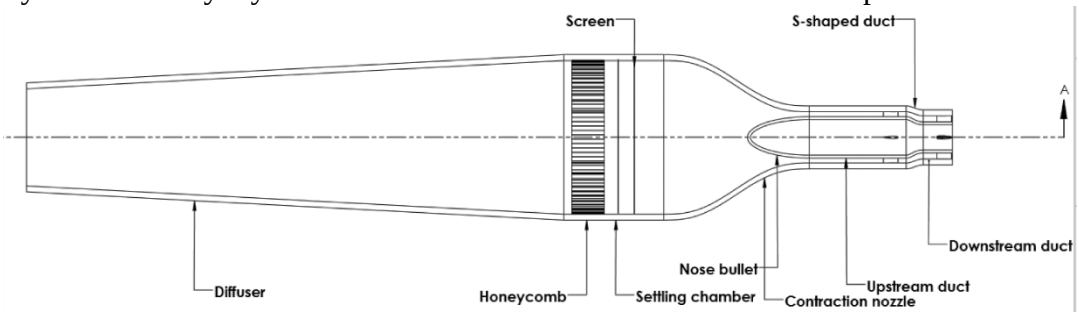

Fig.1 Schematic layout of experimental components

2 Problem Formulation

2.1 Contraction Dimensions

In the present work, the contraction's exit dimensions are based on the S-shaped annular duct. With a contraction ratio of 9, hydraulic diameters of the entrance and the exit are 260.514mm and 86.838mm respectively. As per Bell and Mehta [8], optimum length to height ratio of 0.95 is selected which results in a total length of the computational domain of 352mm ($-52 \leq x \leq 300$) including upstream ($-52 \leq x \leq 0$) and downstream ($300 \leq x \leq 352$) straight portion of 52mm each respectively as shown in Figure 2. The equations of four contraction wall contours are tabulated in Table 1.

Table1. Equations for four investigated contraction (CT) wall contours.

Contraction case	Original Equation	Adopted Equation
CT#1	$Y(x) = H_i - (H_i - H_e)\left[-2\left(\frac{x}{L}\right)^3 + 3\left(\frac{x}{L}\right)^2\right]$	$Y = 130.257 - (130.257 - 43.419)\left[-2\left(\frac{x}{248}\right)^3 + 3\left(\frac{x}{248}\right)^2\right]$
CT#2	$Y(x) = H_i - (H_i - H_e)\left[6\left(\frac{x}{L}\right)^5 - 15\left(\frac{x}{L}\right)^4 + 10\left(\frac{x}{L}\right)^3\right]$	$Y = 130.257 - (130.257 - 43.419)\left[6\left(\frac{x}{248}\right)^5 - 15\left(\frac{x}{248}\right)^4 + 10\left(\frac{x}{248}\right)^3\right]$
CT#3	$Y(x) = H_i - (H_i - H_e)\left[-20\left(\frac{x}{L}\right)^7 + 70\left(\frac{x}{L}\right)^6 - 84\left(\frac{x}{L}\right)^5 + 35\left(\frac{x}{L}\right)^4\right]$	$Y = 130.257 - (130.257 - 43.419)\left[-20\left(\frac{x}{248}\right)^7 + 70\left(\frac{x}{248}\right)^6 - 84\left(\frac{x}{248}\right)^5 + 35\left(\frac{x}{248}\right)^4\right]$
CT#4	$Y(x) = H_e + (H_i - H_e)\left[1 - \frac{1}{x_m^2}\left(\frac{x}{L}\right)^3,\ x < x_m\right]$ $Y(x) = H_e + \left[\frac{(H_i - H_o)}{(1 - x_m)}\left(1 - \frac{x}{L}\right)^3, x > x_m\right]$	$Y = 43.419 + (130.257 - 43.419)\left[1 - \frac{1}{0.5^2}\left(\frac{x}{248}\right)^3,\quad x < 124\right]$ $Y = 43.419 + \left[\frac{(130.257 - 43.419)}{(1 - 0.5)}(1 - 248)^3, x > 124\right]$

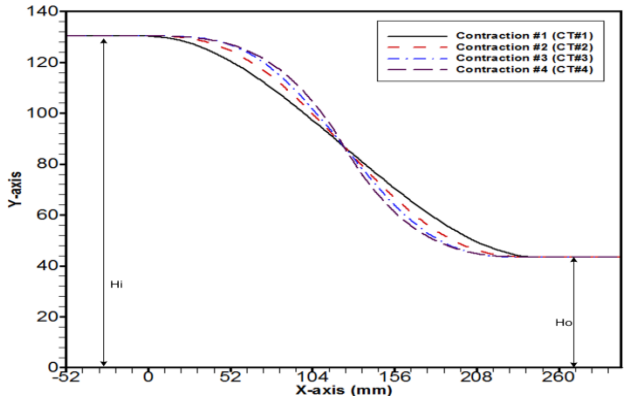

Fig.2 Four investigated contraction wall shapes

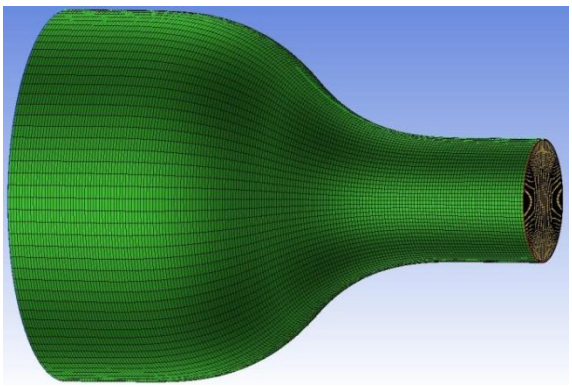

Fig.3 Hexahedral mesh of CT#1case

2.2 Computational Fluid Dynamics Model

To simulate the flow field, it is assumed that flow is steady, three-dimensional, incompressible and turbulent. The Computational domain is designed into Ansys design modeler and meshed into ICEM CFD. Numerical simulation is carried out via FLUENT 15.0 by adopting shear stress transportation (SST) k-ω turbulence model. This model has more strength to predict the flow in the vicinity of the wall more accurately [8]. Pressure-velocity coupling correction is done by the SIMPLE algorithm and second-order upwind scheme is imposed for the momentum, turbulent kinetic energy, and specific dissipation rate. Uniform velocity profile of 7.5 m/s is designated as the inlet boundary condition and 2.94 bar pressure is imposed as the outlet boundary condition whereas No-slip condition is applied on the contraction walls.

In the present case, structured hexahedral mesh of 5.32×10^5 cells are used for all the cases while maintaining the wall distances (y^+) within the boundary layer region below to 1($y^+ \leq 1$) and an example of mesh obtained for the case with CT#1 is shown in Figure 3. To select an optimum mesh size, a grid independent test has been carried out for the case with CT#1. For this, three different mesh sizes are selected and velocity and pressure profiles along the centreline of the contraction are evaluated. Figure 4 and 5 depict that the predicted velocity and pressure profiles are exactly overlapping to each other for all cases hence mesh size of 5.32×10^5 is chosen as the optimum size for the remaining cases.

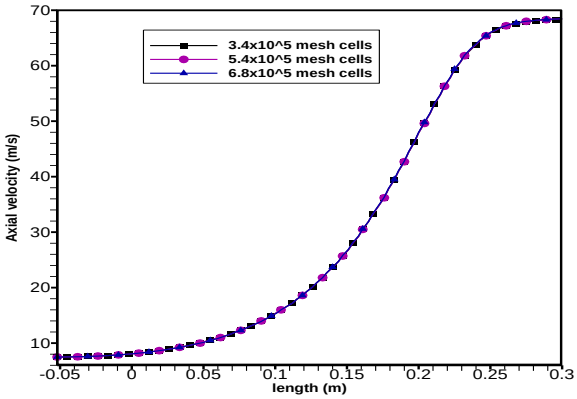

Fig.4 Velocity profiles along centreline for different mesh size

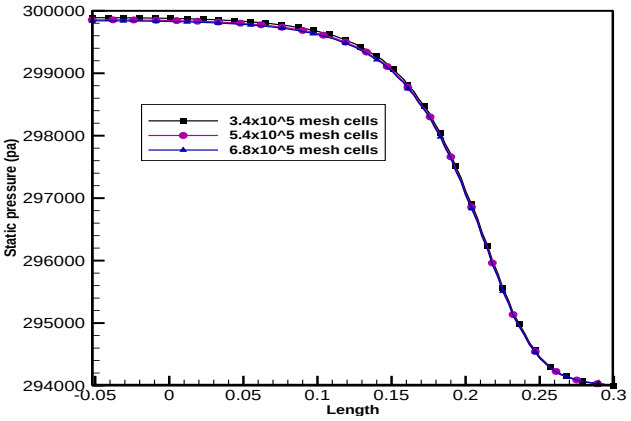

Fig.5 Pressure profiles along centreline for different mesh size

3 Results and Discussion

This section will emphasize the effect of contraction wall shape on the axisymmetric circular cross-sections contractions.

Figure 6 show the static pressure variation along the contraction wall for case of CT#1. Static pressure is the highest at the inlet due to its maximum area and it is gradually decreasing to achieve the minimum value at the outlet. In fact, static pressure and velocity contours for all cases are almost identical and show marginal difference. However, CT#3 requires a higher static upstream pressure to accelerate the flow up to 68 m/s at the contraction exit and as the consequence; it encounters pressure loss of 245.84 Pa which is maximum to the other contractions cases as shown in Table 2. In additions of it, minimum pressure loss is 162.05Pa for the case CT#4. The pressure loss within the contraction could be a cause of higher operating cost.

Table2. Pressure drops along investigated contractions

Case	Inlet total pressure	Outlet total pressure	Loss	% Loss
CT#1	299936.41	299724.28	212.13	0.071
CT#2	299955.41	299725.78	229.63	0.077
CT#3	299972.56	299726.72	245.84	0.082
CT#4	299889.22	299727.16	162.05	0.054

The velocity profiles at the contraction exits are shown in Figure 7. The velocity profile of case CT#1 depicts a thinner boundary layer at the outlet whereas for case CT#4, it is thicker. Higher order equations show thicker boundary layer generation hence have more chance of flow blockage. The core regions of the contraction outlet do not affect by the boundary layer development. The deterioration in uniformity of the flow at the outlet can be expressed in terms of standard deviation in axial velocity at the outlet. The axial velocity standard deviation at the outlet of the contractions is listed in Table 3. The maximum standard deviation is for CT#3 and minimum is achieved for the CT#4.

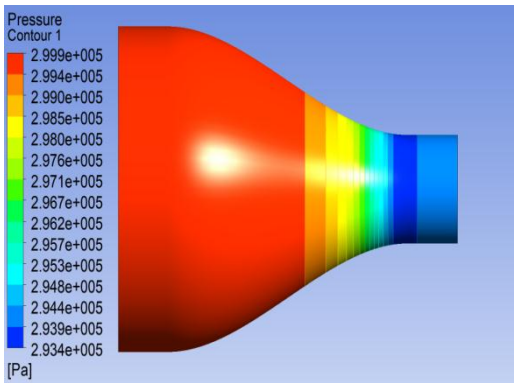

Fig.6 Static pressures contour for CT#1

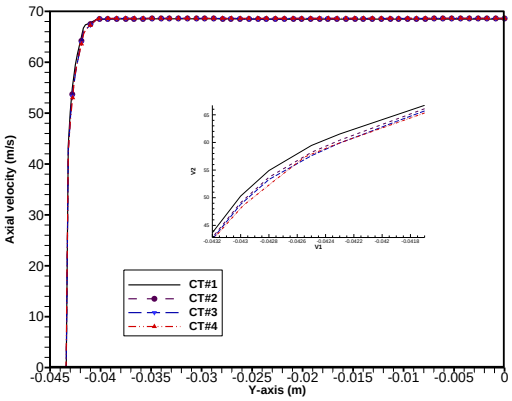

Fig.7. Axial velocity profiles at exit

Table3. Axial velocity standard deviations at outlet

Case	Standard Deviation
CT#1	0.08241
CT#2	0.08818
CT#3	0.08941
CT#4	0.07667

First derivative of wall contour for all the cases are shown by the Figure 8. CT#4 has its highest value at the inflection point (x=124mm) compared to other cases. Hence, it can be concluded that the wall contour of CT#4 changes more rapidly in comparison to the others near the inflection point. Figure 9 presents axial velocity contours for CT#1. At the vicinity of wall boundary layer is developed and gradually increases towards core region.

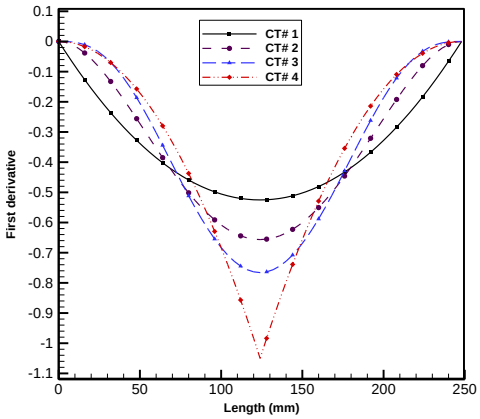

Fig.8 First derivative of wall equations

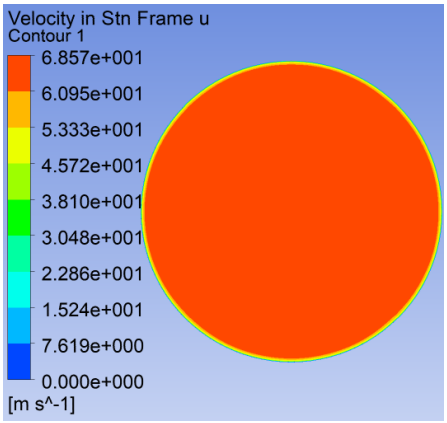

Fig.9 Axial velocity contour at outlet

4 Conclusions

In the present work, computational simulations of contraction of compressor intermediate S-shaped duct facility have been carried out. In order to make a proper understanding about the flow physics of a contraction, four different wall shapes are selected. The main outcomes are highlighted as follows:

1. Different contraction wall shapes result pressure loss within the contraction and the maximum difference between them is about 84Pa. Therefore, the wall shape has the significant role.
2. Maximum value of the first derivatives of a wall shape equation is the highest for a higher order equation which results higher pressure loss for that contraction and less uniformity at the outlet.
3. Higher order equation of wall shape encounters thicker boundary layer as well as higher standard deviation at the outlet of the contraction whereas; Lower order equation results minimum pressure loss.

References

1. Saravanamuttoo, H.I.H., Rogers, G.F.C., Cohen, H.: Gas Turbine Theory (5th Ed.). Pearson Education, Ltd. (2001)

2. Kurzke, J.: Fundamental Differences Between Conventional and Geared Turbofans. In: Proceedings of ASME Turbo Expo 2009: Power for Land, Sea and Air Conference, Orlando, Florida, USA (2009)

3. Norris, Glyn Dominy, R.G.: Flow Through S-Shaped Annular, Inter-Turbine Diffusers, Ph.D. thesis (1998)

4. Fang, Fuh-Min. "A design method for contractions with square end sections." *Journal of Fluids Engineering* 119.2 (1997): 454-458.

5. Mehta, Ravi Datt, and Peter Bradshaw. "Design rules for small low-speed wind tunnels." *The Aeronautical Journal* 83.827 (1979): 443-453.

6. Hernández, Miguel A. González, et al. "Design methodology for a quick and low-cost wind tunnel." *Wind tunnel designs and their diverse engineering applications*. InTech, 2013.

7. Su, Yao-xi. "Flow analysis and design of three-dimensional wind tunnel contractions." *AIAA Journal* 29.11 (1991): 1912-1920.

8. Bell, James H., and Rabindra D. Mehta. "Contraction design for small low-speed wind tunnels." (1988).